THE JOURNAL OF BIOLOGICAL CHEMISTRY VOL. 287, NO. 53, pp. 44289–44300, December 28, 2012

Conservation of Flexible Residue Clusters among Structural and Functional Enzyme Homologues*[S]

Received for publication, July 3, 2012, and in revised form, November 1, 2012 Published, JBC Papers in Press, November 7, 2012, DOI 10.1074/jbc.M112.394866

Donald Gagné[‡1], **Laurie-Anne Charest**[‡1], **Sébastien Morin**[§], **Evgenii L. Kovrigin**[¶], **and Nicolas Doucet**[‡2]

From the [‡]*Institut National de la Recherche Scientifique-Institut Armand-Frappier, Université du Québec, Laval, Quebec H7V 1B7, Canada, the* [§]*Swiss Institute of Bioinformatics and Biozentrum, University of Basel, Klingelbergstrasse 50/70, 4056 Basel, Switzerland, and the* [¶]*Chemistry Department, Marquette University, Milwaukee, Wisconsin 53201*

Background: It remains unclear whether structural homologues rely on similar concerted motions to promote enzyme function.
Results: Ribonuclease homologues display similar, contiguous clustering motions that can be modulated by mutagenesis.
Conclusion: Conformational flexibility can be conserved between distant structural homologues.
Significance: Controlling dynamics to modulate function has broad implications in protein engineering and allosteric drug design.

Conformational flexibility between structural ensembles is an essential component of enzyme function. Although the broad dynamical landscape of proteins is known to promote a number of functional events on multiple time scales, it is yet unknown whether structural and functional enzyme homologues rely on the same concerted residue motions to perform their catalytic function. It is hypothesized that networks of contiguous and flexible residue motions occurring on the biologically relevant millisecond time scale evolved to promote and/or preserve optimal enzyme catalysis. In this study, we use a combination of NMR relaxation dispersion, model-free analysis, and ligand titration experiments to successfully capture and compare the role of conformational flexibility between two structural homologues of the pancreatic ribonuclease family: RNase A and eosinophil cationic protein (or RNase 3). In addition to conserving the same catalytic residues and structural fold, both homologues show similar yet functionally distinct clusters of millisecond dynamics, suggesting that conformational flexibility can be conserved among analogous protein folds displaying low sequence identity. Our work shows that the reduced conformational flexibility of eosinophil cationic protein can be dynamically and functionally reproduced in the RNase A scaffold upon creation of a chimeric hybrid between the two proteins. These results support the hypothesis that conformational flexibility is partly required for catalytic function in homologous enzyme folds, further highlighting the importance of dynamic residue sectors in the structural organization of proteins.

The role of sequence and structure in defining enzyme function is a broadly accepted biological dogma (1). However, structure-function analyses remain very limited in their ability to predict and design new enzyme catalysts. Indeed, information about sequence and structure remains largely insufficient in providing a complete description of the intricate complexities that govern protein folding and enzyme function. Despite recent advancements in predicting folding mechanisms and catalytic function (2, 3), current limitations partly stem from our lack of understanding of the molecular mechanisms that define protein behavior in space and time (*i.e.* as flexible and dynamic macromolecules (4, 5)). Although classical computational design methodologies have typically considered proteins as homogeneously static structures (5), overwhelming theoretical and experimental evidence now advocates a more complex view of their reaction cycle. Among a few other methodologies, NMR relaxation experiments recently uncovered the existence of functionally relevant, low populated conformational states playing essential roles in the thermodynamics of ligand binding, substrate discrimination, active-site reorganization, and product release over the complete time course of an enzyme turnover (6–10). From an enzyme engineering perspective, designing efficient biocatalysts requires the modulation of flexibility events at the atomic scale to exert some control over enzyme function, further validating the need for a better characterization of the motional states found in natural enzymes, thus leading to a superior understanding of their precise role in catalysis (4, 5). In many enzyme systems, conformational exchange has been shown to correlate with the time scale of enzyme turnover, suggesting that flexible networks of concerted residue motions are an integral part of the structure-function relationship in numerous protein architectures (7).

Theoretical studies have postulated the existence of functionally relevant clusters of dynamic residues, which appear to be conserved across evolutionary distant clans of enzyme

* This work was supported in part by Natural Sciences and Engineering Research Council of Canada Discovery Grant RGPIN 402623-2011 (to N. D.) and a Fonds de Recherche du Québec Santé Research Scholar-Junior 1 career award (to N. D.).
[S] This article contains supplemental Figs. S1–S5.
[1] Recipient of a "Fondation Universitaire Armand-Frappier de l'INRS" Ph.D. scholarship.
[2] Supported by the Fonds de Recherche du Québec, Nature et Technologies, Strategic Cluster "Regroupement Québécois de Recherche sur la Fonction, la Structure et l'Ingénierie des Protéines" (PROTEO) and the Fonds de Recherche du Québec Santé (FRQS) Strategic Cluster "Groupe de Recherche Axé sur la Structure des Protéines" (GRASP). To whom correspondence should be addressed: INRS-Institut Armand-Frappier, Université du Québec, 531 Blvd. des Prairies, Laval, Québec H7V 1B7, Canada. Tel.: 450-687-5010 (ext. 4212); Fax: 450-686-5501; E-mail: nicolas.doucet@iaf.inrs.ca.

superfamilies (11) and among members of the same enzyme fold (12). Although these studies put forth compelling evidence suggesting that enzyme function is at least partly controlled by conformational exchange, the experimental validation of such hypotheses remains largely unexplored. Although the role of flexibility in enzyme function has been amply demonstrated on a case-by-case basis (7, 9), it is yet unknown whether residue motions on multiple time scales are evolutionary traits conserved among structurally and functionally similar homologues.

Having been studied for more than 50 years as a *de facto* protein model for biochemical and biophysical analyses (13–15), ribonucleases represent an excellent model system to investigate the evolutionary and dynamic processes that regulate catalytic function among enzyme homologues. RNase A is the founding member of the mammalian and vertebrate superfamily that bears its name, which comprises an extensive network of functionally distinct enzymes sharing invariant structural and catalytic elements (16). These enzymes all catalyze the transphosphorylation and subsequent hydrolysis of single-stranded RNA molecules (Fig. 1), but they also carry broad and yet relatively uncharacterized biological activities. Initial sequencing of the human genome identified eight canonical members of this family (RNases 1–8), all of which preserve the same catalytic triad and display the analogous kidney-shaped tertiary fold of RNase A (17). These structurally similar enzymes catalyze such diversified activities as neurotoxicity, angiogenesis, immunosuppressivity, or anti-pathogenicity while still preserving varying degrees of ribonucleolytic activity. Although they do not all degrade RNA with the same catalytic efficiency, human ribonucleases require the strict conservation of important catalytic residues to perform their non-catalytic function (16). Interestingly, one of the few exceptions to this rule is eosinophil cationic protein (ECP,[3] or RNase 3), a human canonical member for which a functional active site is not always required for biological function (18), much like in RNase 7 (19). ECP has been the subject of many studies over the past few years, mainly because of its potential use as an antibiotic and as a cytotoxic agent (20). Although its biological function remains unclear, ECP has been shown to display antibacterial, neurotoxic, helminthotoxic, antiviral, and cytotoxic activities, some of them independent of its ribonucleolytic activity (18).

Short and long range concerted residue motions occurring on the time scale of k_{cat} ($\sim 10^{-3}$ s) have been shown to correlate with substrate-to-product conversion and rearrangement in a number of divergent enzyme systems and thus are postulated to be essential for optimal enzyme function (6, 7). Motions on the faster picosecond-to-nanosecond (ps-ns) time scale have also been shown to be important in enzyme function, namely by destabilizing the ground state and affecting the rates of barrier crossing associated with chemical exchange (21). We and others have shown that RNase A requires concerted millisecond (ms) dynamics for efficient catalysis through motions involving a distant loop (loop 1, residues 14–26) located more than 20 Å away from the reactive center (22). During turnover, the flexible loop 1 propagates ms motions to the active site through a highly conserved pair of hydrogen-bonded residues (His^{48}-Thr^{82}), which are located on the adjacent β1 and β4 strands (23). These molecular motions are transmitted over a length scale of more than 20 Å from loop 1 to active site residues Thr^{45} and Asp^{83} (also located in β1 and β4), providing important pyrimidine interactions with RNA ligands during catalysis (23, 24). As was demonstrated by mutagenesis (22, 23, 25) and unnatural amino acid modifications (24), this concerted dynamic network is essential for optimal catalysis in RNase A, acting by modulating the rate-limiting step of the reaction (product release). Although the dynamically important residue pair His^{48}-Thr^{82} is 86% conserved in the mammalian and vertebrate ribonuclease superfamily (23), ECP is one of only two human ribonucleases lacking this important interaction, coinciding with a steep decrease in ribonucleolytic activity (18).

Based on these observations, it is tempting to verify whether evolutionarily conserved motional networks between homologous ribonucleases could partially account for their divergent catalytic activities. In the present study, we aimed at validating whether highly homologous structural and functional ribonucleases catalyzing the same transphosphorylation reaction also display conserved dynamic behaviors both on the fast ps-ns and the slower microsecond-to-millisecond (μs-ms) time scales. We challenge this hypothesis by investigating the conformational exchange and the conservation of dynamic clusters between ECP and RNase A, two structural homologues of the ribonuclease superfamily. We used NMR relaxation dispersion, model-free analysis, and titration experiments to show that both enzymes display similar millisecond dynamic residue clusters near their active sites, with relatively rigid and homogeneous backbone fluctuations on the ps-ns time frame. Interestingly, although motional clusters are structurally conserved between the two homologues, their respective global rates of conformational exchange (k_{ex}) vary significantly. As predicted by the absence of the functionally dynamic His^{48}-Thr^{82} residue pair in ECP, this enzyme lacks the aforementioned loop 1-β1-β4 network of coupled residue motions previously shown to be involved in the modulation of product release in RNase A. Additionally, this functionally essential network can be eliminated in RNase A by swapping loop 1 for that of ECP in the RNase A_{ECP} chimera (22).

Our current motional investigation demonstrates that both ECP and a chimeric hybrid between RNase A and ECP (RNase A_{ECP} (22)) show very similar dynamic behaviors, further highlighting the possibility of using mutagenesis to control residue flexibility and function through the dynamic conversion of one enzyme (RNase A) into another (ECP). Finally, our conformational investigation of ECP confirms previous RNase A observations suggesting that this fold can be dynamically divided into several independent regional flexible subdomains (or dynamic clusters).

The current study represents one of the very few experimental validations of similar conformational exchange in structurally related enzymes (26, 27) and the first to compare similar mesophile homologues, confirming theoretical observations

[3] The abbreviations used are: ECP, eosinophil cationic protein; ms, millisecond; ps-ns, picosecond-to-nanosecond; μs-ms, microsecond-to-millisecond; HSQC, heteronuclear single-quantum coherence; CPMG, Carr-Purcell-Meiboom-Gill.

suggesting that specific motions can be evolutionarily conserved within and among structurally similar protein folds. The present work also demonstrates the importance of controlling millisecond dynamics to modulate protein function, a central concept with broad implications in protein engineering and allosteric drug design (4, 5, 28, 29).

EXPERIMENTAL PROCEDURES

Cloning, Expression, and Purification—*Escherichia coli* codon-optimized sequences of ECP and RNase A (GenScript) were subcloned into NdeI/HindIII-digested expression vector pET22b(+) (EMD Biosciences) and transformed into *E. coli* BL21(DE3). ^{15}N-Labeled samples were prepared by growing *E. coli* BL21(DE3) in M9 minimal medium, and enzymes were purified as described by Boix (18) (ECP) and Doucet *et al.* (22) (RNase A). Protein concentration was determined using an extinction coefficient of 17,460 $\text{M}^{-1}\,\text{cm}^{-1}$ (9,800 $\text{M}^{-1}\,\text{cm}^{-1}$) for ECP (18) (RNase A (30)).

Solution NMR Experiments—All NMR experiments were recorded at 298 K on samples containing 0.2–0.7 mM ^{15}N-labeled ECP in 15 mM sodium acetate, 10% $^{2}H_2O$, pH 5.0 or containing 0.7 mM ^{15}N-labeled RNase A in 5 mM MES-NaOH, 7 mM NaCl, 0.01% NaN_3, 10% $^{2}H_2O$, pH 6.4. NMR experiments were carried out on Varian (Agilent) 500- and 800-MHz NMR spectrometers equipped with triple-resonance cold probes and pulsed field gradients. Backbone resonance assignments for apo-ECP were taken from the Biological Magnetic Resonance Data Bank (entry 15757) and further confirmed with a ^{1}H-^{15}N total correlation spectroscopy heteronuclear single-quantum coherence (TOCSY-HSQC) experiment.

Relaxation Dispersion Experiments (μs-ms Motions)—Backbone amide ^{15}N CPMG relaxation dispersion experiments were acquired on apo and saturated enzyme complexes using published sequences (31) and methods (22). Interleaved two-dimensional spectra were collected in a constant time manner with τ_{cp} CPMG repetition delays of 0.625, 0.714 (×2), 1.0, 1.25, 1.67, 2.0, 2.50 (×2), 3.33, 5.0, and 10 ms, using a total relaxation period of 40 ms. All NMR spectra were processed using NMRPipe (32) and in-house CPMG scripts and analyzed with Sparky (33). Global residue fits and model analyses were performed by fitting 500- and 800-MHz CPMG dispersion data to the full single-quantum CPMG equation (34) using GraphPad Prism 5.

Fast Time Scale Motions (ps-ns)—^{15}N-R_1, ^{15}N-R_2 and steady state heteronuclear NOE experiments were performed in an interleaved fashion at 500 MHz, as described previously (35, 36). The R_1 experiments were performed with relaxation delays of 10, 50, 100 (×2), 200, 350, 700, 1100, and 1400 ms. The R_2 experiments were performed with relaxation delays of 10, 30, 50 (×2), 70, 90, 110, and 130 ms. The motional parameters on the faster ps-ns time scale were analyzed by fitting the NMR spin relaxation rates to the model-free formalism (reviewed in Ref. 37), using the methodology for the dual optimization of the model-free parameters and the global diffusion tensor proposed by d'Auvergne (38) and implemented in the program *relax* 2.1.0 (38, 39). The crystallographic structure of free ECP was used as starting coordinates (PDB entry 1QMT), and hydrogen atoms were added in DS Visualizer 3.5 (Accelrys). Values for the ^{15}N chemical shift anisotropy and N–H bond length were set at −172 ppm and 1.02 Å, respectively. Model selection for each residue and diffusion tensors was tested, optimized, and selected using the Akaike information criterion as described in the *relax* manual. Errors were obtained from 500 Monte Carlo simulations.

NMR Titration Experiments—Freshly prepared 3′-UMP and 5′-AMP ligands were dissolved in ECP or RNase A NMR buffers. ^{1}H-^{15}N sensitivity-enhanced HSQC experiments were acquired at 800 MHz using spectral widths (points) of 1600 Hz (256) and 7000 Hz (8192) in the t_1 and t_2 dimensions, respectively. ^{1}H-^{15}N HSQC spectra were collected for titration points of ligand-enzyme ratios of 0, 0.174, 0.393, 0.691, 1.31, 2.71, 6, and 12. The pH was maintained constant by the addition of 0.01 M HCl, when necessary.

NMR Line Shape Analysis—Analysis of NMR line shapes originating from titrations of ECP with 3′-UMP and 5′-AMP ligands was performed using the NMR line shape analysis module of the Integrative Data Analysis Platform (40). The one-dimensional data sets for fitting were obtained as slices through the fast exchange peaks in ^{1}H-^{15}N HSQC spectra using Sparky (33) with a custom Python extension (41). The one-dimensional NMR line shape was simulated using Bloch-McConnell equations for a spin exchanging between two magnetic environments as described earlier (42, 43). The line shapes were optimized to fit the experimental data by varying the thermodynamic equilibrium constant and the dissociation rate constant as well as the frequency of the bound complex using the Integrative Data Analysis Platform code implemented in MATLAB (MathWorks). The S.E. values were estimated from fitting of multiple line shape data sets generated with the addition of the Gaussian noise to the spectral intensities and solution concentrations. The uncertainty of the best-fit parameters was determined by the boundaries enclosing 95% of all best-fit results collected in the runs with Gaussian perturbations. The Integrative Data Analysis Platform software is available upon request from Evgenii L. Kovrigin.

RESULTS

Ligand Binding Interactions in ECP and RNase A—The structural and functional binding differences between ECP and RNase A were assessed by NMR titration experiments using the 3′-UMP and 5′-AMP ligands (Fig. 1, *b* and *c*). 3′-UMP and 5′-AMP are single nucleotide homologues of the end products of the UpA dinucleotide RNA substrate, providing good structural assessments of the individual ribonuclease subsites involved in substrate binding to the active site cavity in both enzymes. Ligands were individually titrated in ^{15}N-labeled proteins, and binding was followed by measuring chemical shift variations observed in ^{1}H-^{15}N HSQC spectra until saturation was reached. Affinities of 3′-UMP and 5′-AMP binding to ECP were estimated using line shapes observed in the ^{1}H-^{15}N HSQC titration experiments (41–43). Observation of ligand binding to the cognate sites in ECP was complicated by the apparent secondary binding events observed in both titrations, probably due to weak affinity of the nucleotides to a second nonspecific site. To estimate affinity of the binding interaction with the cognate site in the 3′-UMP data sets, we selected residues that

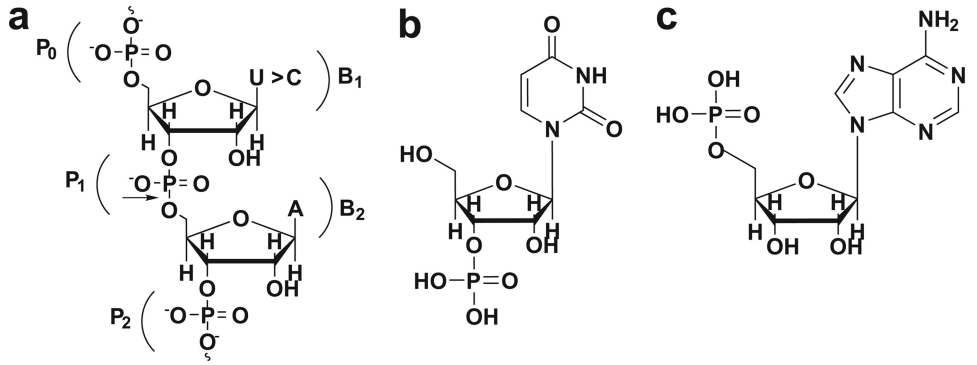

FIGURE 1. **Substrates and products of a ribonuclease reaction.** *a*, schematic representation of a single-stranded RNA molecule binding to the active site of ECP. Phosphate and base binding subsites for RNA substrates are defined as P_n and B_n, of which the P_{0-2} and B_{1-2} subsites are shown (18). The phosphodiester bond scission occurs at the P_1 subsite (*arrow*) and is universally catalyzed by two strictly conserved histidine residues: His^{15} and His^{128} (ECP numbering). In ECP, uracil is preferred over cytosine in the B_1 subsite (U > C), a preference that is reversed in RNase A (C > U). Adenosine is almost universally required at the B_2 subsite. *b*, schematic representation of the uracil-3′-monophosphate ligand (*3′-UMP*). *c*, schematic representation of the adenosine-5′-monophosphate ligand (*5′-AMP*).

only responded to the main binding event in ECP (*i.e.* Val^{125} and Val^{127}) (supplemental Fig. S1). The 5′-AMP binding has much weaker contribution from the second binding process, so residues demonstrating the most significant shifts were analyzed (His^{15}, Ala^{110}, and His^{128}). Despite significant scatter of the global dissociation rate constants obtained in the individual fitting, the equilibrium dissociation constant (K_d) was accurately estimated in all cases (supplemental Fig. S1). Therefore, global fitting to obtain K_d within each group was performed on ECP, resulting in dissociation constants of 340 ± 30 μM for 5′-AMP and 460 ± 100 μM for 3′-UMP (Table 1).

In both enzymes, the 3′-UMP and 5′-AMP nucleotides preferentially bind to the B_1 and B_2 subsites of the active site cavity, respectively. This provided a unique opportunity to characterize distinct atomic interactions involved in ligand discrimination in both structural homologues (Fig. 2). A total of 12 residues showed significant (>0.1 ppm) ^1H-^{15}N weighted average chemical shift variations upon 3′-UMP binding to ECP, relative to 17 residues in RNase A (Fig. 2, *a* and *b*). Although the chemically affected residues are mostly located in the vicinity of the B_1 subsite and are directly involved in binding and/or catalysis in RNase A (*e.g.* His^{12}, Lys^{41}, Thr^{45}, and His^{119}) (Fig. 2*b*), their functional equivalents in ECP (His^{15}, Lys^{39}, Thr^{42}, and His^{128}) do not show significant chemical shift perturbations upon 3′-UMP binding (Fig. 2*a*). If 3′-UMP does bind to the B1 subsite of ECP as expected, this would illustrate that the high sequence conservation of active site residues in the two homologues does not translate into similar pyrimidine recognition, partly accounting for the significantly reduced binding affinity of 3′-UMP in ECP (Table 1). Pyrimidine contacts with Thr^{45} and Asp^{83} are required for optimal product release in RNase A (24). However, no Asp^{83} equivalent can be found in ECP, and Thr^{42} (the Thr^{45} equivalent) is completely unaffected by 3′-UMP binding. Additionally, residues displaying important chemical shifts upon 3′-UMP binding are scattered throughout the ECP structure, contrasting with the relatively bundled group of clustering residues in RNase A (Fig. 2*b*).

Based on their motional behavior (see below) and secondary structure elements (44), the two structural homologues were divided into four distinct regional residue clusters encompassing loop 4 (cluster 1), the β2 sheet (cluster 2), the β1 sheet and adjacent loop 1 (cluster 3), and loops 2 and 6 (cluster 4) (Fig. 3). Interestingly, the contiguous residues displaying important chemical shift variations upon pyrimidine binding to RNase A (Thr^{45}, Phe^{46}, Thr^{82}, Thr^{100}, Gln^{101}, all part of cluster 3) also show important conformational exchange on the millisecond time scale and are known to be involved in the propagation of motions between loop 1 and the active site during turnover (22, 23). Coupled to the chemical shift differences induced by 3′-UMP binding, this observation strongly suggests that long scale millisecond motions connecting the active site to loop 1 (cluster 3) are involved in the binding/release of pyrimidine ligands in RNase A. Although long scale chemical shift variations are also observed in ECP upon pyrimidine binding (*e.g.* residues Gln^{58}, Arg^{75}, and Arg^{77}, located 20.2, 18.0, and 14.7 Å away from the ligand, respectively), residues of cluster 3 in ECP are not similarly responsive, and no contiguous residue network is affected upon ligand binding to this enzyme (Fig. 2). Additionally, residues of the ECP cluster 3 (β1-sheet and adjacent loop 1) are almost completely devoid of significant chemical shift perturbations upon 3′-UMP binding to the B_1 subsite, suggesting that concerted long range interactions linking loop 1 to the active site are not functionally important in ECP.

Purine binding to the B_2 subsite also yields important chemical shift differences between these two structural homologues. Whereas the chemical environment of only 4 residues is significantly perturbed upon 5′-AMP binding to ECP, 14 residues are affected when this ligand binds to RNase A (Fig. 2, *c* and *d*). The magnitude in the ^1H-^{15}N weighted average chemical shift variations is also stronger in RNase A than ECP. Only the immediate vicinity of the B_2 subsite is chemically affected in presence of 5′-AMP in ECP, including the important catalytic residues

TABLE 1
Binding affinities of 3′-UMP and 5′-AMP to RNase A and ECP

	K_d 3′-UMP	K_d 5′-AMP
	μM	μM
RNase A	9.7 ± 0.9[a]	124.0 ± 0.9[b]
ECP	460 ± 100[c]	340 ± 30[c]

[a] Taken from Ref. 65.
[b] Taken from Ref. 66.
[c] Estimated from NMR line shape analysis (see "Experimental Procedures").

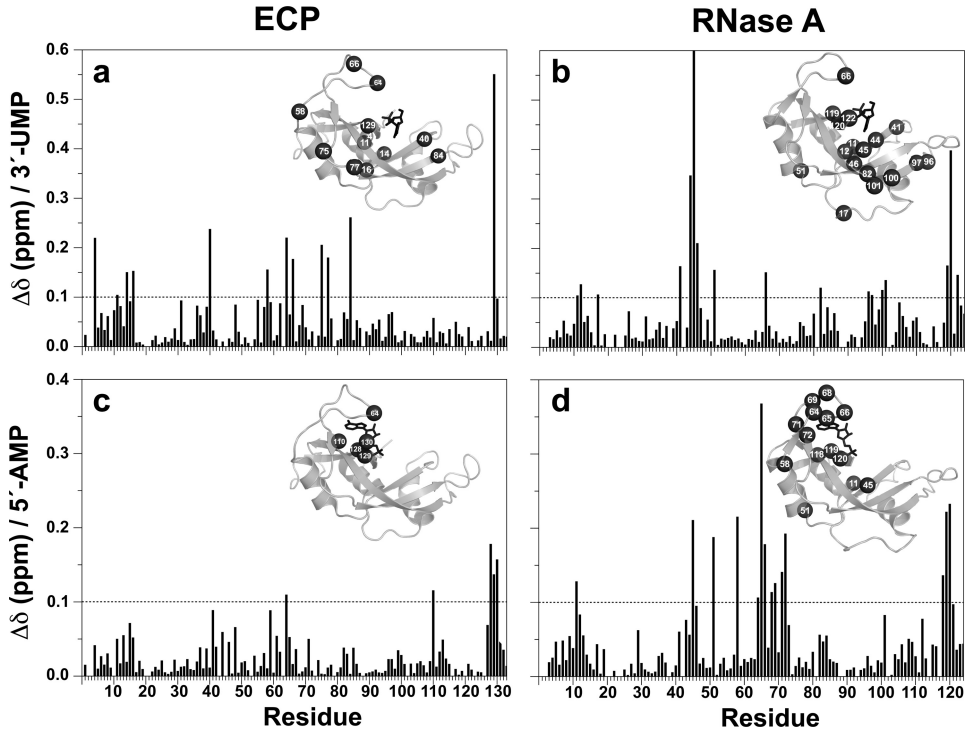

FIGURE 2. **^{1}H-^{15}N chemical shift variations induced by 3′-UMP and 5′-AMP binding to ECP and RNase A.** Weighted average chemical shift differences (Δδ) for 3′-UMP (*a* and *b*) and 5′-AMP (*c* and *d*) are mapped on the primary sequence of ECP (*a* and *c*) and RNase A (*b* and *d*). The ^{1}H-^{15}N weighted average composite chemical shift differences (Δδ) were calculated between free and ligand-saturated enzymes according to the equation (67), $\Delta\delta\ (\text{ppm}) = ((\Delta\delta^2_{HN} + \Delta\delta^2_{N}/25)/2)^{1/2}$. The position of 3′-UMP and 5′-AMP (*black sticks*) is displayed on the three-dimensional structure of RNase A (PDB entry 1O0N) and is predicted on ECP (PDB entry 1H1H) based on a structural overlay with RNase A. *Black spheres* represent residues with $\Delta\delta > 0.1$ ppm.

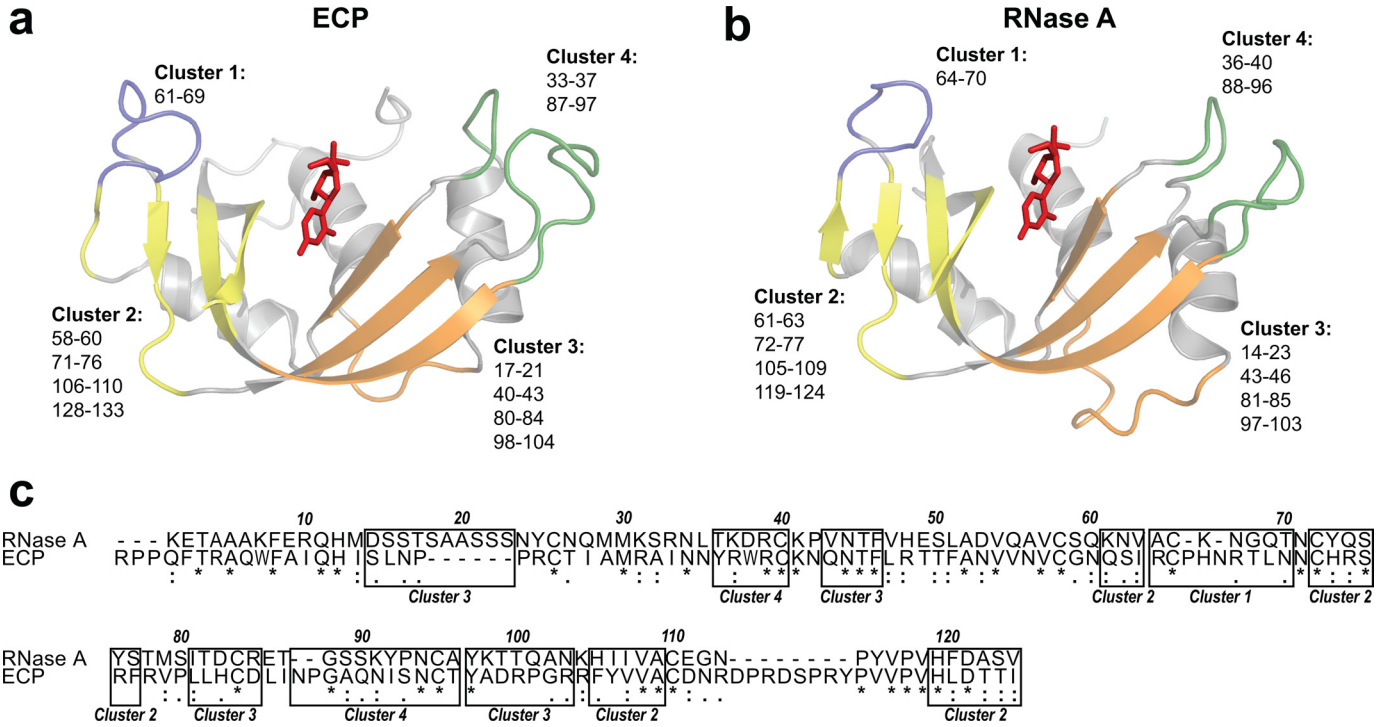

FIGURE 3. **Dynamic residue clusters in ECP and RNase A.** The two ribonuclease homologues are divided into four distinct residue clusters covering the following secondary structure elements (44): loop 4 (cluster 1, *purple*), β2-sheet (cluster 2, *yellow*), β1-sheet with adjacent loop 1 (cluster 3, *orange*), and loops 2 and 6 (cluster 4, *green*). The four *color-coded* clusters are highlighted on the three-dimensional structure of ECP (PDB entry 1H1H) (*a*) and RNase A (PDB entry 1O0N) (*b*), with encompassed residues listed. The 3′-UMP ligand is shown in *red*. *c*, Expresso (68) sequence alignment of ECP and RNase A showing the position of conserved residues and secondary structure elements forming the dynamic clusters. Sequence numbering is that of RNase A.

His^{64} and His^{128}. Whereas His^{128} is required for the hydrolytic step of the reaction, His^{64} (located in loop 4) directly interacts with P_0 during turnover and is thought to act as the functional equivalent to Lys^{66} in RNase A (45). The most striking differences observed upon 5′-AMP binding to ECP and RNase A occur for residues of clusters 1 and 2 (Fig. 3), more specifically for residues in loop 4 (cluster 1). Although residues of loop 4 show considerable chemical shift variations upon 5′-AMP binding to RNase A, only His^{64} is affected when this purine binds to ECP. This loop faces the active site and acts as an arm that holds the purine ligand in position (Fig. 2*d*). Interestingly, loop 4 is the only dynamic cluster experiencing conformational exchange in both the free forms of ECP and RNase A, albeit with distinct conformational exchange rates (see below).

Fast Time Scale Analysis (ps-ns)—Although most proteins interact and catalyze reactions on a time frame much slower than nanoseconds, the kinetics and thermodynamics underlying such larger conformational motions may rely on faster time scale dynamics (21). In an effort to decipher the importance of such fast motions in ECP and to compare them with the previously characterized ps-ns motions in RNase A (35), we fitted the ^{15}N-R_1, ^{15}N-R_2 and heteronuclear NOE spin relaxation data to the new approach for the dual optimization of the model-free parameters and the global diffusion tensor proposed by d'Auvergne and Gooley (38, 39). The spin relaxation behavior of 112 of the 121 non-proline residues of ECP could be reliably quantitated. Residues Phe^{43}, Arg^{45}, Asn^{53}, Gln^{58}, Asn^{70}, Arg^{73}, Phe^{76}, Cys^{83}, and Leu^{129} were removed from the analysis because of low signal intensity and/or spectral overlapping and/or because they were absent from the ^{1}H-^{15}N HSQC. The average values of the relaxation rates are $R_1 = 1.13 \pm 0.13$ s^{-1} and $R_2 = 14.04 \pm 1.78$ s^{-1}, and NOE = 0.478 ± 0.71 (supplemental Fig. S2). Much like in RNase A, the ECP heteronuclear NOE values at the N and C terminus of the protein are similar to those in the rest of the protein. This was expected because of the structural similarity in the protein architecture, which relies on the N-terminal helix and C-terminal sheet packing for binding and activity (35).

The model-free calculated order parameters (S^2) are used to characterize the amplitude of the internal motions of the ^{1}H-^{15}N vector on the ps-ns time scale and thus provide a measure of atomic scale residue flexibility on this particular time frame (46–48). As a result, a completely unrestricted ^{1}H-^{15}N bond vector would show an S^2 value of 0, whereas a fully rigid one would display an order parameter of 1. The generalized S^2 parameters determined from model-free fitting are plotted as a function of residue number in Fig. 4. The calculated order parameters are relatively high and uniform across the sequence, much like with RNase A (35). However, the average value of $S^2 = 0.740 \pm 0.052$ indicates that ECP is a bit more flexible than the very rigid RNase A on the ps-ns time scale, which displays an average $S^2 = 0.910 \pm 0.051$ (35). Interestingly, the catalytic residue Lys^{38} in ECP, which is strictly conserved among pancreatic RNases, displays one of the highest order parameters in the protein ($S^2 = 0.848 \pm 0.026$), along with its very rigid neighbor Asn^{39} ($S^2 = 0.907 \pm 0.055$). Lys^{38} is thought to be involved in the stabilization of the excess negative charge on the phosphoryl oxygens in the transition state during RNA cleavage

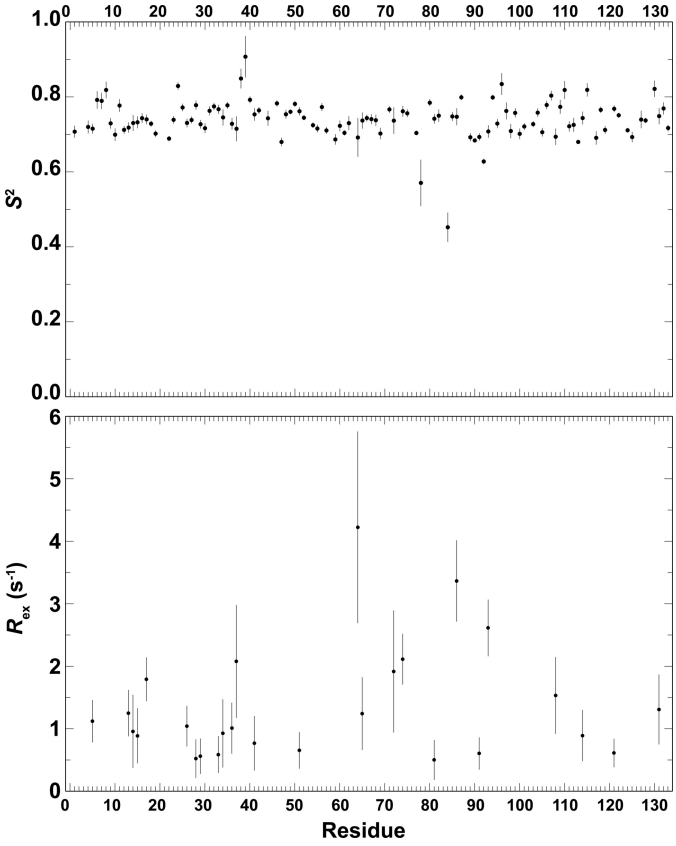

FIGURE 4. **Model-free calculated S^2 and R_{ex} parameters plotted on the sequence of ECP.** The generalized order parameters (S^2) provide a measure of atomic scale flexibility of the ^{1}H-^{15}N bond vector on the ps-ns time scale. The predicted R_{ex} parameter accounts for contributions to R_2 that potentially describe motions occurring on the slower μs-ms time scale.

(15), which may require rigidity in ECP. On the contrary, the two most flexible residues, Val^{78} ($S^2 = 0.571 \pm 0.062$) and Asp^{84} ($S^2 = 0.452 \pm 0.039$), are at the beginning and the end of the β2 strand, respectively. Neither was shown to play any particular role in enzyme function.

For a number of residues that do not fit to simple calculation models, an R_{ex} exchange parameter is calculated to achieve an adequate fit to the model-free analysis. This R_{ex} parameter accounts for contributions to R_2 that potentially describe motions occurring on the slower μs-ms time scale (Fig. 4). Much like with RNase A, a large number of residues throughout the ECP sequence require the addition of this exchange contribution (26 of the 112 residues analyzed), suggesting the existence of motions occurring on the slower μs-ms time scale in this enzyme. This observation is in line with our slow time scale analysis of ECP performed by ^{15}N CPMG (see below), most notably for residues of loop 4 (cluster 1; Fig. 3), which display some of the most important R_{ex} values in the protein (Fig. 4). Interestingly, the highest R_{ex} observed is for residue His^{64} ($R_{ex} = 4.22 \pm 1.53$ s^{-1}), the structural equivalent to Lys^{66} in RNase A, which is also one of the most flexible residues of RNase A on the millisecond time scale (Fig. 5*c*). Overall, although ECP is a bit more flexible than RNase A on the ps-ns time frame, both enzymes show relatively rigid and homogeneous backbone fluctuations on this particular time scale, in addi-

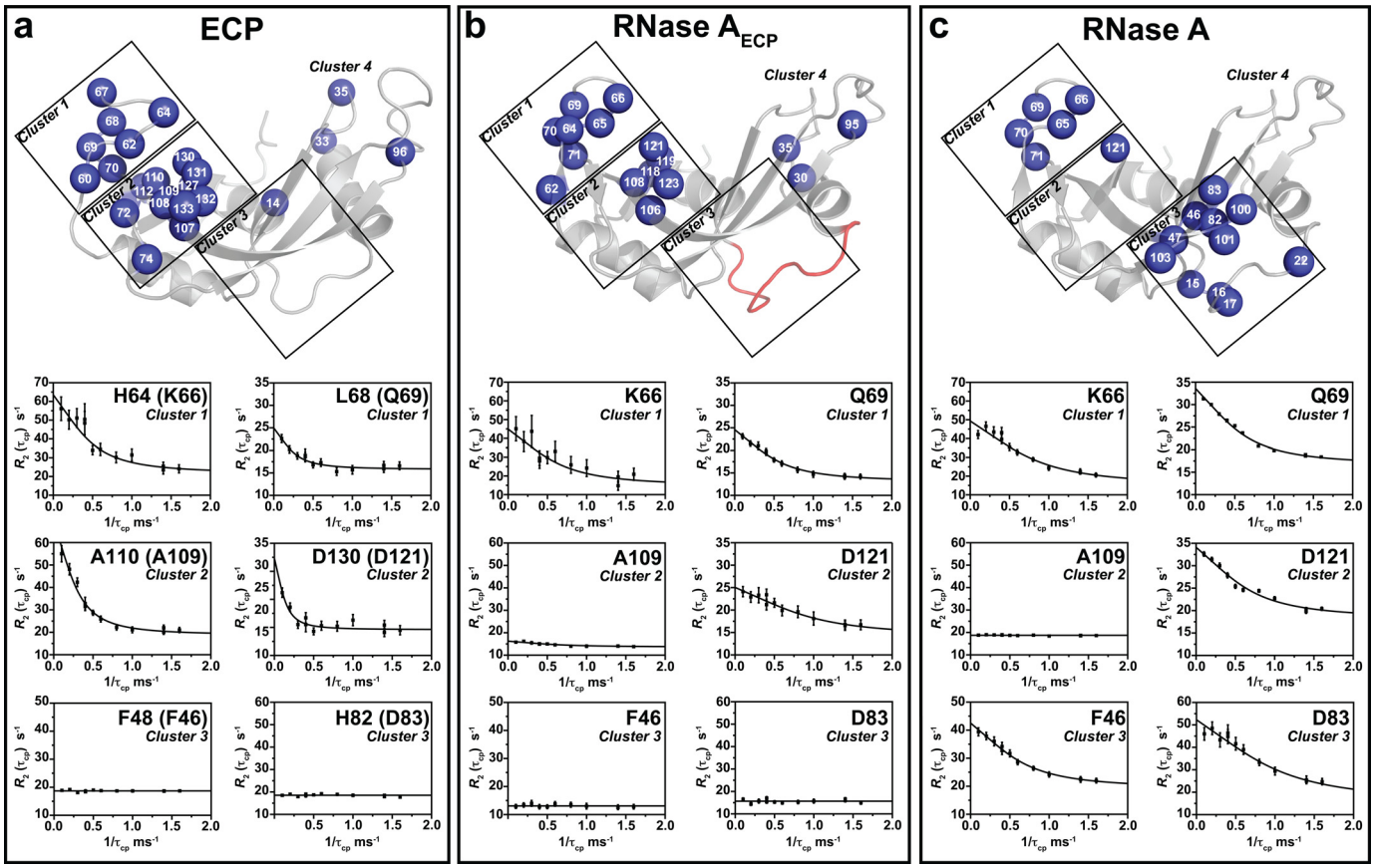

FIGURE 5. **Conformational exchange is confined to four independent yet contiguous dynamic clusters in structural and functional ribonuclease homologues.** Conformational exchange was investigated in the apo forms of ECP, RNase A, and the chimeric hybrid RNase A_{ECP}, in which the RNase A loop 1 (^{14}DSSTSAASSSNY^{25}, in *red*) was replaced by that of ECP (^{17}SLNPPR^{22}, ECP numbering) (22). Catalytic time scale (ms) residue motions were probed using ^{15}N CPMG relaxation dispersion experiments at 500 and 800 MHz (298 K) for the apo forms of ECP (*a*), RNase A_{ECP} (*b*), and RNase A (*c*). Residues were considered for further analysis only if the difference in measured R_2 (ΔR_2 ($1/\tau_{cp}$)) values at fast (τ_{cp} = 0.625 ms) and slow (τ_{cp} = 10 ms) pulsing rates was greater than 2 s^{-1}, similar to previous reports (22, 35). *Blue spheres* represent residues displaying ^{15}N CPMG dispersion with ΔR_2 ($1/\tau_{cp}$) > 2 s^{-1}. Residues are highlighted on the three-dimensional structure of ECP (PDB entry 1H1H) (*a*) and RNase A (PDB entry 1O0N) (*b* and *c*). Representative relaxation dispersion curves (800 MHz, 298 K) are shown for structurally equivalent positions of ECP (RNase A) found in cluster 1 (His^{64} (Lys^{66}) and Leu^{68} (Gln^{69})), cluster 2 (Ala^{110} (Ala^{109}) and Asp^{130} (Asp^{121})), and cluster 3 (Phe^{48} (Phe^{46}) and His^{82} (Asp^{83})). Flexible residues experiencing ^{1}H-^{15}N bond vector motions on the millisecond time scale display a relaxation dispersion curve, whereas residues with no motion on this particular time frame display flat relaxation profiles. Swapping loop 1 of RNase A with that of ECP converts the dynamic clusters of the former into those of the latter. RNase A_{ECP} data were taken from Ref. 22.

tion to similar flexible residue sectors on the millisecond time scale (see below).

Conserved Networks of Flexible Millisecond Residue Clusters—We investigated the apo and ligand-bound millisecond motions experienced by both structural homologues using solution NMR relaxation dispersion experiments (^{15}N CPMG) (10). ^{15}N CPMG experiments allow the characterization of an equilibrium exchange process experienced by the ^{1}H-^{15}N bond vector by recording the transverse relaxation rate constant, R_2, as a function of τ_{cp}, an interpulse delay in the CPMG pulse train (49). ^{15}N CPMG experiments thus enable the detection of millisecond dynamics in proteins caused by internal conformational exchange, ligand binding, and/or the chemical reaction (for reviews, see Refs. 9 and 50–52). When R_2 values are plotted as a function of $1/\tau_{cp}$, the characteristic dispersion of R_2 values reveals residues experiencing conformational exchange on the millisecond time scale (Fig. 5). On the contrary, ^{15}N nuclear spins that do not experience motions on this particular time frame do not show any dispersion (flat line profiles). In addition to this qualitative assessment, the fitted relaxation dispersion curves can further be quantitatively analyzed to extract structural information of the excited state (differences in chemical shifts, $\Delta\omega$) as well as population dynamics (exchange rates (k_{ex}) and equilibrium populations ($p_A p_B$)) (see Ref. 49 and references therein).

Our results demonstrate that ECP and RNase A reveal four clusters of dynamic residues closely mapping the structural clusters shown in Fig. 3. We also observed that conformational exchange in these clusters is significantly different between the two proteins (Fig. 5). In both homologues, similar contiguous residues experiencing conformational exchange interact with their structural neighbors to form bundles of cross-talking networks that transfer millisecond motions over structurally distinct clusters and subdomains of the protein. Although ECP and RNase A display different catalytic activities and binding properties, these two structural homologues nevertheless constrain millisecond dynamics to these four dynamic clusters instead of displaying randomly scattered ms dynamics throughout the protein structure. These localized dynamic clusters suggest that conformational exchange may have evolved through the formation of confined and contiguous networks of coupled motions to support common function and/or that ms dynamics

may play distinct roles in the biological function of these structural and functional homologues. This clustering of ms dynamics into contiguous yet independent motional sectors may thus serve as a point of comparison to analyze functional differences between enzyme homologues.

A direct comparison of the dynamic clusters between RNase A and ECP indicates that some residue clusters experiencing conformational exchange in one protein homologue are almost entirely silenced in the other. This can be observed for the core residues of clusters 2 and 3. For instance, 12 residues of cluster 2 show considerable conformational exchange in ECP (Fig. 5*a*), a region that is almost completely devoid of ms dynamics in RNase A (Fig. 5*c*). Simultaneous fitting of the all-time scale, two-state Carver-Richards equation (34) to the spin relaxation data obtained at 500 and 800 MHz for all ECP residues of cluster 2 yielded a global exchange rate constant (k_{ex}) of 728 ± 104 s^{-1}. Inversely, although cluster 3 motions are entirely absent from ECP, 11 nearly contiguous residues linking the active site to loop 1 in RNase A show a global k_{ex} of 1,438 ± 125 s^{-1} (Fig. 5*c*). Cluster 1 is the only protein sector showing important conformational exchange in both structural homologues. Relaxation dispersion is observed for 5 and 6 residues of loop 4 in RNase A and ECP, respectively. Whereas the global exchange rate of loop 4 (k_{ex} = 1548 ± 82 s^{-1}) parallels the product release and catalytic rates in RNase A ($k_{off} = k_{cat}$), the global exchange rate for loop 4 is more than 3 times slower in ECP (k_{ex} = 504 ± 44 s^{-1}) and appears to be unrelated to k_{cat} (18). Interestingly, cluster 3 in RNase A encompasses the same long scale residues experiencing chemical shift variations upon pyrimidine binding (Fig. 2*b*), in line with previous hypotheses linking motions of this cluster to product release in RNase A (22–25). However, efforts to correlate free and 3′-UMP- or 5′-AMP-bound ^{15}N chemical shift variations (Δδ ppm) with ^{15}N chemical shift differences between the major and the minor excited state obtained from ^{15}N CPMG (Δω) remained inconclusive (supplemental Fig. S3). In an ideal case, *i.e.* when the excited state of the enzyme corresponds to the product-bound form obtained by a shift in the reaction equilibrium (in this case saturation with 3′-UMP or 5′-AMP product analogues), one should expect a perfect linear correlation between the ^{15}N chemical shift differences of the NMR titrations (Δδ ppm) and the Δω ppm obtained from ^{15}N CPMG. The absence of such linear correlation implies additional perturbations caused by the arrival of the ligands and/or implies that the conformational exchange we observe by ^{15}N CPMG is unrelated to transitions between free and product-bound states in both ECP and RNase A. The observation of exchange at certain sites may be reflecting or providing a measure of ground state destabilization that is essential for catalysis but unrelated to the functional importance of the excited state in product release. The integrity of such motional networks nevertheless remains critical for optimal enzyme catalysis in both homologues, as was previously demonstrated elsewhere (22–25, 41) and in the present study (see below).

The RNase A_{ECP} Chimera; Translating RNase A Dynamics into Those of ECP—Some of us have previously shown that cluster 3 residues in RNase A propagate motions from loop 1 (residues 14–24) to β strands 1 and 4, both of them containing the important active site residues Thr^{45} and Asp^{83} involved in RNA pyrimidine stabilization at the active site (22–25). These motions correlate to those of the distant loop 1 and affect the rate-limiting step of RNase A catalysis by limiting the rate of product release. This was demonstrated by creating a chimeric hybrid between RNase A and ECP in which loop 1 in the former is replaced by loop 1 of the latter (generating the RNase A_{ECP} chimera), affecting both the millisecond dynamics and activity of the enzyme (22). Not only is loop 1 conformationally restrained and much shorter in ECP than in RNase A (6 residues in the former *versus* 12 in the latter); ECP also lacks the important His^{48}-Thr^{82} residue pair that we showed to be essential for the propagation of ms motions in this dynamic cluster (23). As mentioned above, cluster 3 residues are completely devoid of conformational exchange in ECP (Fig. 5*a*), highlighting a different dynamic landscape in this protein.

Originally not apparent from the first chimera study (22), one of the most impressive observations of the global dynamic comparison between ECP and RNase A is the motional similarity between ECP and the swapped mutant of RNase A (RNase A_{ECP}; Fig. 5, *a* and *b*). Despite conserving 90% sequence identity with RNase A, the RNase A_{ECP} chimera almost perfectly mirrors the ms dynamics of ECP. Indeed, the conformational exchange of cluster 3 residues is completely dampened in the RNase A_{ECP} hybrid. Conversely, millisecond dynamics are acquired for contiguous residues in cluster 2 (Fig. 5*b*), a sector that is almost completely devoid of ms motions in RNase A (Fig. 5*c*). Even a few residues of cluster 4 now experience conformational exchange in this chimeric hybrid, a protein cluster that is otherwise very rigid in RNase A.

Consequently, replacing the distant loop 1 in RNase A not only reduces ligand binding by 1 order of magnitude (22); it also affects the entire conformational flexibility of the enzyme by translating the dynamic landscape of WT RNase A into that observed in WT ECP. These results demonstrate that mutagenesis can be used to selectively modulate conformational exchange in proteins, a prerequisite to exert efficient control over motional residue networks affecting function in protein engineering and drug design applications (4, 5, 29).

Relationship between Ligand Binding and Internal Dynamics— To clarify the effect of ligand binding on the collective dynamics of each structural homologue, we also performed ^{15}N CPMG experiments in the presence of saturating concentrations of 3′-UMP and 5′-AMP (Fig. 6). For both enzymes, ligand-bound complexes show that conformational exchange is still segregated to the same four clusters as those observed for the unbound forms. Using relaxation dispersion measurements, it may be possible to show how internal conformational equilibrium is shifted by the addition of a ligand. This "population shift" (6) has been demonstrated in RNase A by comparing frequency differences between major and minor dynamic states between the free and ligand-bound enzyme (41). This analysis requires very high quality relaxation data because the frequency difference of exchanging conformers is most difficult to obtain in the fast exchange regime (53). To attempt this analysis in ECP, we performed global fittings of residues in each dynamic individual cluster (1 and 2) such that k_{ex} and populations were shared while the frequency difference was individual for each

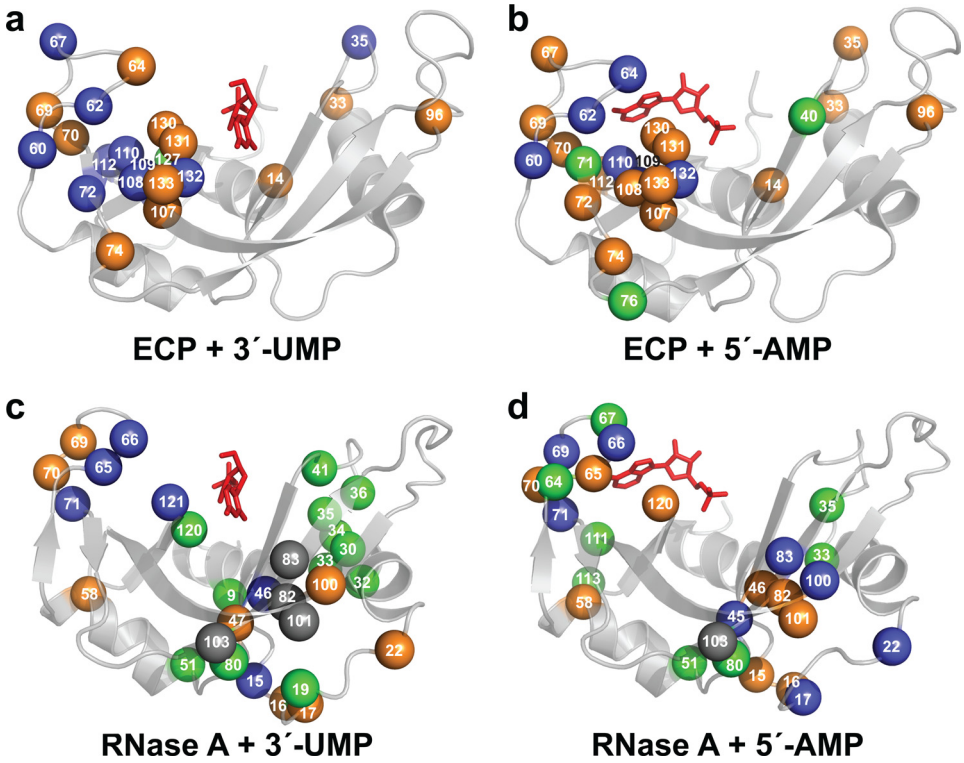

FIGURE 6. **Conformational exchange induced by 3′-UMP and 5′-AMP binding to ECP and RNase A.** Catalytic time scale (ms) residue dynamics were probed using ^{15}N CPMG relaxation dispersion experiments for 3′-UMP-bound (*a* and *c*) and 5′-AMP-bound (*b* and *d*) forms of ECP (*a* and *b*) and RNase A (*c* and *d*). *Blue spheres*, residues showing ^{15}N CPMG dispersion profiles with a $\Delta R_2\,(1/\tau_{cp}) > 2\ s^{-1}$; *orange spheres*, residues showing no conformational exchange relative to the apo form (*i.e.* dampened ms dynamics upon ligand binding); *green spheres*, residues gaining conformational exchange ($\Delta R_2\,(1/\tau_{cp}) > 2\ s^{-1}$) upon ligand binding; *gray spheres*, assigned residues in the apo form that cannot be assigned in the ligand-bound form due to line broadening. Residues are highlighted on the three-dimensional structure of ECP (PDB entry 1H1H) and RNase A (PDB entry 1O0N). The 3′-UMP and 5′-AMP ligands are shown in *red*.

residue. The results were filtered on the basis of the coefficient of determination ($R^2 > 0.9$) to ensure that only good fits were used in the analysis. Due to spectral overlap induced by ligand binding and variable data quality, only residues Cys^{62} and Thr^{67} (cluster 1) were available in the free and ligand-bound forms for comparison. For Cys^{62}, we determined that the frequency difference between major and minor conformers was in the 95% confidence interval of 320–450 s^{-1} for apo-ECP and 300–530 s^{-1} for the ECP-3′-UMP complex. For Thr^{67}, the corresponding ranges for the same complexes were 180–240 and 190–290 s^{-1}, respectively. Similarity of the frequency differences between conformations in the free and bound forms of ECP may indicate that the same type of population shift is induced by the ligand in ECP as the one observed in the earlier RNase A report (41).

Our NMR results nevertheless point to significant motional distinctions in the behavior of ECP and RNase A upon ligand binding. The most striking effect is the gaining and dampening of conformational exchange in the aforementioned motional clusters regardless of the RNA ligand investigated. Indeed, whereas 3′-UMP and 5′-AMP considerably rigidify the ECP structure upon binding (Fig. 6, *a* and *b*), the opposite is true for RNase A, for which an increase in the total amount of residues displaying relaxation dispersion can be observed (Fig. 6, *c* and *d*). A total of 11 (8) and 14 (9) residues rigidify upon 3′-UMP and 5′-AMP binding to ECP (RNase A), respectively (supplemental Figs. S4 and S5). However, the increase in conformational exchange upon ligand binding is considerably more pronounced in RNase A than ECP. This is particularly true for the 3′-UMP complex (Fig. 6*c*), in which ligand binding induces conformational exchange for all residues of α2 facing the hydrophobic core of the enzyme (residues 25–34, cluster 4). Globally, only 1 and 3 residues gain ms dynamics when 3′-UMP and 5′-AMP bind to ECP, respectively. This number jumps to 12 and 8 residues when the same two ligands bind to RNase A. The increase in RNase A ms dynamics upon ligand binding is also supported by the disappearance of several ^{1}H-^{15}N HSQC backbone resonances due to line broadening in the hinge region of cluster 3 (Fig. 6, *c* and *d*, *gray spheres*). Overall, these observations are consistent with the previously suggested ligand-dependent induction of hinge motions between the two β-sheets (54), a distinctive feature of RNase A that is undetectable in ECP.

The comparison between residues experiencing nitrogen chemical shift variations and the effect they exert on conformational exchange upon ligand binding also yields interesting distinctions between ECP and RNase A (supplemental Figs. S4 and S5). For instance, the strictly conserved catalytic lysine (Lys^{41} in RNase A, Lys^{38} in ECP) is thought to be involved in the stabilization of the excess negative charge on the phosphoryl oxygens in the transition state during RNA cleavage (15). Surprisingly, although the flexible Lys^{41} in RNase A shows significant chemical shift variations in the presence of 3′-UMP, Lys^{38} is not at all affected by ligand binding and does not show any conformational exchange in ECP (supplemental Fig. S4). Although Lys^{41} gains conformational exchange in the RNase A-nucleotide

complex, this result is not observed in ECP. This different binding and dynamic behavior for such an important catalytic residue may partly explain the important differences observed in the catalytic rates of these two RNases (18), which is also supported by the restricted ^{1}H-^{15}N bond vector of Lys^{38} on the ps-ns time scale. Also, it is interesting to point out that Phe^{46}, one of the most critical aromatic residues for RNase A stability and folding (55–57), is flexible in both the apo and 3′-UMP-bound forms of RNase A (supplemental Fig. S4). Although very highly conserved in the RNase family and positioned in the exact same orientation, no such flexibility is observed for Phe^{43} in ECP. These observations suggest that very similar functional homologues may still use local dynamics for very different purposes in defining function and stability.

DISCUSSION

Most of the work investigating the importance of conserved functional dynamics among enzyme family homologues was historically achieved through computational analyses. These studies typically use coarse-grained models, such as normal mode analysis, to infer catalytic time scale motional similarities between protein folds (58). Generally, these studies also involve the direct comparison of simulated data with crystallographically resolved and/or NMR-resolved enzymes in apo and ligand-bound forms, inferring dynamic information through, but not limited to, residual dipolar coupling measurements and/or Debye-Waller factors (*B*-factors) (59). The latter provides a rough approximation of residue flexibility in protein crystals, albeit with no clear definition of dynamic time scale.

Theoretical studies have delivered a breadth of relevant information on slow time scale conservation of functionally relevant motions in many enzyme families and protein folds, including, but not limited to, the amino acid kinase family (59), aspartate proteases (11), oxidoreductases, and peptidyl-prolyl isomerases (12). Nonetheless, experimental validation of such theoretical observations remains elusive, and very few experimental studies have yet provided a clear portrait of catalytically relevant dynamic conservation between structural and functional protein homologues. The present work partly provides such validation by showing that two members of the pancreatic-like ribonuclease family sharing similar catalytic mechanisms and protein folds also retain similar ps-ns dynamics and conformational exchange on the ms time scale. The present study also validates the existence of dynamic clusters, similar to the evolutionary sectors of Ranganathan and co-workers (60, 61), which transcend the classical definition of primary, secondary, or tertiary protein architectures. We observe that millisecond dynamic clusters are sequestered into distinct protein subdomains and, as previously suggested, appear to be structurally encoded and "fine tuned" by the protein fold (Fig. 5) (60). The dynamic subdomain (cluster 3) that transfers millisecond motions essential to product release in RNase A is absent from ECP. Despite having the same dynamic cluster architecture as that of RNase A, experimental evidence illustrates that ECP is a more conformationally restrained homologue on the ms time scale.

Previous theoretical studies have suggested the existence of collective motions in the pancreatic-like ribonuclease family using molecular dynamics simulations (62, 63). Until very recently, such analyses remained confined to the very fast time scales that can be probed by MD simulations (ps-ns), a time frame that is still very far from enzyme turnover (ms). To overcome such a barrier, Ramanathan and Agarwal (12) recently used quasiharmonic analysis to model large scale conformational fluctuations occurring on slower time scales in this enzyme family, providing the most complete theoretical comparison of slow dynamics between ribonuclease homologues so far. Focusing on the motional comparison of three pancreatic-like ribonuclease homologues from humans, bovines, and rats, the authors show remarkable interspecies similarities in the slow motions of surface loops and distal motifs in this enzyme family, observations that transcend sequence identity. The present investigation offers the first experimental validation of the existence of such theoretical networks between two members of the pancreatic ribonuclease family.

The conservation of clustering sectors of coevolving residues among family members and functional homologues has been suggested as a potentially important structural determinant defining biological function in proteins. Ranganathan and co-workers (60) have used statistical coupling analyses of sequence alignments to argue that the classical hierarchy of primary, secondary, tertiary, and quaternary structures used to define protein architecture remains largely insufficient to explain the three-dimensional cooperativity observed between coevolving residues among protein homologues. Much like the confined assemblies of dynamic residue clusters highlighted in the present study, the investigators argue that non-random correlations in the physical connectivity between coevolving groups of residues in the three-dimensional structure of the S1A serine protease family underlie the biological function of its members, a property they also observed in the PDZ, PAS, Src homology 2, and Src homology 3 domain families (60). These groups of coevolving residues, termed sectors (60, 61), show striking physical connectivity in the three-dimensional structure of protein families while completely transcending classical subdivisions of primary, secondary, or tertiary subdomain architectures. These sectors, which show stark three-dimensional similarity with the dynamic clusters observed in the present work, are shown to be structurally independent and confined to functional regions among the serine protease family, encompassing residues involved in binding or catalysis (60). Most interestingly, Ranganathan and co-workers (61) also observe a direct correlation between these coevolving sectors and the networks of residues undergoing conformational fluctuations associated with enzyme catalysis in dihydrofolate reductase. Similar to the experimentally characterized clusters in the present work, the authors show that dynamic motions associated with catalysis in dihydrofolate reductase extend well beyond the active site environment, dynamically connecting surface sites on both ends of the enzyme through long range networks of dynamic residues that cross-talk on the catalytic time scale (61).

The present study, coupled to our previous demonstration that RNase A relies on a 20-Å communication link between the active site and loop 1 for optimal catalysis (22–25), suggests that the Ranganathan sectors of coevolving residues may represent a

conserved mechanism to initiate allosteric regulation on protein surfaces (61, 64). We experimentally uncovered a similar architecture between two homologues of the ribonuclease fold, lending further support to the potential evolutionary conservation of motional networks defining function in protein families. Systematic analysis of correlations between dynamics and function for important protein families is likely to provide novel insights into the structure-function-flexibility relationship that defines protein architectures. This knowledge is required for successful *de novo* enzyme design (4, 5, 29) as well as for the development of new allosteric drugs (28).

Acknowledgments—We thank Gennady Khirich and J. Patrick Loria (Yale University) for helpful discussions and for providing part of the NMR assignments of RNase A and RNase A_{ECP}. We also thank Tara Sprules and Sameer Al-Abdul-Wahid from the Québec/Eastern Canada High Field NMR Facility for excellent NMR technical assistance as well as Éric Déziel and Claude Guertin (Institut National de la Recherche Scientifique) for kind generosity.

REFERENCES

1. Branden, C., and Tooze, J. (1999) *Introduction to Protein Structure*, 2nd Ed., Garland Science, New York
2. Eiben, C. B., Siegel, J. B., Bale, J. B., Cooper, S., Khatib, F., Shen, B. W., Players, F., Stoddard, B. L., Popovic, Z., and Baker, D. (2012) Increased Diels-Alderase activity through backbone remodeling guided by Foldit players. *Nat. Biotechnol.* **30,** 190–192
3. Siegel, J. B., Zanghellini, A., Lovick, H. M., Kiss, G., Lambert, A. R., St Clair, J. L., Gallaher, J. L., Hilvert, D., Gelb, M. H., Stoddard, B. L., Houk, K. N., Michael, F. E., and Baker, D. (2010) Computational design of an enzyme catalyst for a stereoselective bimolecular Diels-Alder reaction. *Science* **329,** 309–313
4. Baker, D. (2010) An exciting but challenging road ahead for computational enzyme design. *Protein Sci.* **19,** 1817–1819
5. Lassila, J. K. (2010) Conformational diversity and computational enzyme design. *Curr. Opin. Chem. Biol.* **14,** 676–682
6. Ma, B., and Nussinov, R. (2010) Enzyme dynamics point to stepwise conformational selection in catalysis. *Curr. Opin. Chem. Biol.* **14,** 652–659
7. Henzler-Wildman, K., and Kern, D. (2007) Dynamic personalities of proteins. *Nature* **450,** 964–972
8. Baldwin, A. J., and Kay, L. E. (2009) NMR spectroscopy brings invisible protein states into focus. *Nat. Chem. Biol.* **5,** 808–814
9. Doucet, N. (2011) Can enzyme engineering benefit from the modulation of protein motions? Lessons learned from NMR relaxation dispersion experiments. *Protein Pept. Lett.* **18,** 336–343
10. Loria, J. P., Berlow, R. B., and Watt, E. D. (2008) Characterization of enzyme motions by solution NMR relaxation dispersion. *Acc. Chem. Res.* **41,** 214–221
11. Carnevale, V., Raugei, S., Micheletti, C., and Carloni, P. (2006) Convergent dynamics in the protease enzymatic superfamily. *J. Am. Chem. Soc.* **128,** 9766–9772
12. Ramanathan, A., and Agarwal, P. K. (2011) Evolutionarily conserved linkage between enzyme fold, flexibility, and catalysis. *PLoS Biol.* **9,** e1001193
13. Cuchillo, C. M., Nogués, M. V., and Raines, R. T. (2011) Bovine pancreatic ribonuclease. Fifty years of the first enzymatic reaction mechanism. *Biochemistry* **50,** 7835–7841
14. Marshall, G. R., Feng, J. A., and Kuster, D. J. (2008) Back to the future. Ribonuclease A. *Biopolymers* **90,** 259–277
15. Raines, R. T. (1998) Ribonuclease A. *Chem. Rev.* **98,** 1045–1066
16. Dyer, K. D., and Rosenberg, H. F. (2006) The RNase A superfamily. Generation of diversity and innate host defense. *Mol. Divers.* **10,** 585–597
17. Sorrentino, S. (2010) The eight human "canonical" ribonucleases. Molecular diversity, catalytic properties, and special biological actions of the enzyme proteins. *FEBS Lett.* **584,** 2194–2200
18. Boix, E. (2001) Eosinophil cationic protein. *Methods Enzymol.* **341,** 287–305
19. Huang, Y. C., Lin, Y. M., Chang, T. W., Wu, S. J., Lee, Y. S., Chang, M. D., Chen, C., Wu, S. H., and Liao, Y. D. (2007) The flexible and clustered lysine residues of human ribonuclease 7 are critical for membrane permeability and antimicrobial activity. *J. Biol. Chem.* **282,** 4626–4633
20. Boix, E., and Nogués, M. V. (2007) Mammalian antimicrobial proteins and peptides. Overview on the RNase A superfamily members involved in innate host defence. *Mol. Biosyst.* **3,** 317–335
21. Jarymowycz, V. A., and Stone, M. J. (2006) Fast time scale dynamics of protein backbones. NMR relaxation methods, applications, and functional consequences. *Chem. Rev.* **106,** 1624–1671
22. Doucet, N., Watt, E. D., and Loria, J. P. (2009) The flexibility of a distant loop modulates active site motion and product release in ribonuclease A. *Biochemistry* **48,** 7160–7168
23. Doucet, N., Khirich, G., Kovrigin, E. L., and Loria, J. P. (2011) Alteration of hydrogen bonding in the vicinity of histidine 48 disrupts millisecond motions in RNase A. *Biochemistry* **50,** 1723–1730
24. Watt, E. D., Rivalta, I., Whittier, S. K., Batista, V. S., and Loria, J. P. (2011) Reengineering rate-limiting, millisecond enzyme motions by introduction of an unnatural amino acid. *Biophys. J.* **101,** 411–420
25. Watt, E. D., Shimada, H., Kovrigin, E. L., and Loria, J. P. (2007) The mechanism of rate-limiting motions in enzyme function. *Proc. Natl. Acad. Sci. U.S.A.* **104,** 11981–11986
26. Butterwick, J. A., Loria, J. P., Astrof, N. S., Kroenke, C. D., Cole, R., Rance, M., and Palmer, A. G., 3rd. (2004) Multiple time scale backbone dynamics of homologous thermophilic and mesophilic ribonuclease HI enzymes. *J. Mol. Biol.* **339,** 855–871
27. Henzler-Wildman, K. A., Lei, M., Thai, V., Kerns, S. J., Karplus, M., and Kern, D. (2007) A hierarchy of timescales in protein dynamics is linked to enzyme catalysis. *Nature* **450,** 913–916
28. Lee, G. M., and Craik, C. S. (2009) Trapping moving targets with small molecules. *Science* **324,** 213–215
29. Davey, J. A., and Chica, R. A. (2012) Multistate approaches in computational protein design. *Protein. Sci.* **21,** 1241–1252
30. Sela, M., and Anfinsen, C. B. (1957) Some spectrophotometric and polarimetric experiments with ribonuclease. *Biochim. Biophys. Acta* **24,** 229–235
31. Loria, J. P., Rance, M., and Palmer, A. G., 3rd (1999) A relaxation-compensated Carr-Purcell-Meiboom-Gill sequence for characterizing chemical exchange by NMR spectroscopy. *J. Am. Chem. Soc.* **121,** 2331–2332
32. Delaglio, F., Grzesiek, S., Vuister, G. W., Zhu, G., Pfeifer, J., and Bax, A. (1995) NMRPipe. A multidimensional spectral processing system based on UNIX pipes. *J. Biomol. NMR* **6,** 277–293
33. Goddard, T. D., and Kneller, D. G. (2008) *Sparky*, version 3, University of California, San Francisco, CA
34. Carver, J. P., and Richards, R. E. (1972) A general two-site solution for the chemical exchange produced dependence of T_2 upon the Carr-Purcell pulse separation. *J. Magn. Reson.* **6,** 89–105
35. Cole, R., and Loria, J. P. (2002) Evidence for flexibility in the function of ribonuclease A. *Biochemistry* **41,** 6072–6081
36. Doucet, N., Savard, P. Y., Pelletier, J. N., and Gagné, S. M. (2007) NMR investigation of Tyr^{105} mutants in TEM-1 β-lactamase. Dynamics are correlated with function. *J. Biol. Chem.* **282,** 21448–21459
37. Morin, S. (2011) A practical guide to protein dynamics from ^{15}N spin relaxation in solution. *Prog. Nucl. Magn. Reson. Spectrosc.* **59,** 245–262
38. d'Auvergne, E. J., and Gooley, P. R. (2008) Optimisation of NMR dynamic models II. A new methodology for the dual optimisation of the model-free parameters and the Brownian rotational diffusion tensor. *J. Biomol. NMR* **40,** 121–133
39. d'Auvergne, E. J., and Gooley, P. R. (2008) Optimisation of NMR dynamic models I. Minimisation algorithms and their performance within the model-free and Brownian rotational diffusion spaces. *J. Biomol. NMR* **40,** 107–119
40. Kovrigin, E. L. (2012) NMR line shapes and multi-state binding equilibria. *J. Biomol. NMR* **53,** 257–270
41. Kovrigin, E. L., and Loria, J. P. (2006) Enzyme dynamics along the reaction coordinate. Critical role of a conserved residue. *Biochemistry* **45,**

2636–2647
42. Kaplan, J. I., and Fraenkel, G. (1980) *NMR of Chemically Exchanging Systems*, Academic Press, Inc., New York
43. Rao, B. D. (1989) Nuclear magnetic resonance line-shape analysis and determination of exchange rates. *Methods Enzymol.* **176,** 279–311
44. Mallorquí-Fernández, G., Pous, J., Peracaula, R., Aymamí, J., Maeda, T., Tada, H., Yamada, H., Seno, M., de Llorens, R., Gomis-Rüth, F. X., and Coll, M. (2000) Three-dimensional crystal structure of human eosinophil cationic protein (RNase 3) at 1.75 Å resolution. *J. Mol. Biol.* **300,** 1297–1307
45. Boix, E., Leonidas, D. D., Nikolovski, Z., Nogués, M. V., Cuchillo, C. M., and Acharya, K. R. (1999) Crystal structure of eosinophil cationic protein at 2.4 Å resolution. *Biochemistry* **38,** 16794–16801
46. Lipari, G., and Szabo, A. (1982) Model-free approach to the interpretation of nuclear magnetic-resonance relaxation in macromolecules II. Analysis of experimental results. *J. Am. Chem. Soc.* **104,** 4559–4570
47. Lipari, G., and Szabo, A. (1982) Model-free approach to the interpretation of nuclear magnetic-resonance relaxation in macromolecules I. Theory and range of validity. *J. Am. Chem. Soc.* **104,** 4546–4559
48. Mandel, A. M., Akke, M., and Palmer, A. G., 3rd. (1995) Backbone dynamics of *Escherichia coli* ribonuclease HI. Correlations with structure and function in an active enzyme. *J. Mol. Biol.* **246,** 144–163
49. Manley, G., and Loria, J. P. (2012) NMR insights into protein allostery. *Arch. Biochem. Biophys.* **519,** 223–231
50. Kay, L. E. (2005) NMR studies of protein structure and dynamics. *J. Magn. Reson.* **173,** 193–207
51. Palmer, A. G., 3rd (2001) NMR probes of molecular dynamics. Overview and comparison with other techniques. *Annu. Rev. Biophys. Biomol. Struct.* **30,** 129–155
52. Palmer, A. G., 3rd (2004) NMR characterization of the dynamics of biomacromolecules. *Chem. Rev.* **104,** 3623–3640
53. Kovrigin, E. L., Kempf, J. G., Grey, M. J., and Loria, J. P. (2006) Faithful estimation of dynamics parameters from CPMG relaxation dispersion measurements. *J. Magn. Reson.* **180,** 93–104
54. Vitagliano, L., Merlino, A., Zagari, A., and Mazzarella, L. (2002) Reversible substrate-induced domain motions in ribonuclease A. *Proteins* **46,** 97–104
55. Chatani, E., Nonomura, K., Hayashi, R., Balny, C., and Lange, R. (2002) Comparison of heat- and pressure-induced unfolding of ribonuclease A. The critical role of Phe^{46} which appears to belong to a new hydrophobic chain-folding initiation site. *Biochemistry* **41,** 4567–4574
56. Kadonosono, T., Chatani, E., Hayashi, R., Moriyama, H., and Ueki, T. (2003) Minimization of cavity size ensures protein stability and folding. Structures of Phe^{46}-replaced bovine pancreatic RNase A. *Biochemistry* **42,** 10651–10658
57. Vila, R., Benito, A., Ribó, M., and Vilanova, M. (2009) Mapping the stability clusters in bovine pancreatic ribonuclease A. *Biopolymers* **91,** 1038–1047
58. Bahar, I., and Rader, A. J. (2005) Coarse-grained normal mode analysis in structural biology. *Curr. Opin. Struct. Biol.* **15,** 586–592
59. Marcos, E., Crehuet, R., and Bahar, I. (2010) On the conservation of the slow conformational dynamics within the amino acid kinase family. NAGK the paradigm. *PLoS Comput. Biol.* **6,** e1000738
60. Halabi, N., Rivoire, O., Leibler, S., and Ranganathan, R. (2009) Protein sectors. Evolutionary units of three-dimensional structure. *Cell* **138,** 774–786
61. Reynolds, K. A., McLaughlin, R. N., and Ranganathan, R. (2011) Hot spots for allosteric regulation on protein surfaces. *Cell* **147,** 1564–1575
62. Merlino, A., Vitagliano, L., Ceruso, M. A., Di Nola, A., and Mazzarella, L. (2002) Global and local motions in ribonuclease A. A molecular dynamics study. *Biopolymers* **65,** 274–283
63. Merlino, A., Vitagliano, L., Ceruso, M. A., and Mazzarella, L. (2003) Subtle functional collective motions in pancreatic-like ribonucleases. From ribonuclease A to angiogenin. *Proteins* **53,** 101–110
64. Gunasekaran, K., Ma, B., and Nussinov, R. (2004) Is allostery an intrinsic property of all dynamic proteins? *Proteins* **57,** 433–443
65. Fisher, B. M., Schultz, L. W., and Raines, R. T. (1998) Coulombic effects of remote subsites on the active site of ribonuclease A. *Biochemistry* **37,** 17386–17401
66. Doucet, N., Jayasundera, T. B., Simonović, M., and Loria, J. P. (2010) The crystal structure of ribonuclease A in complex with thymidine-3′-monophosphate provides further insight into ligand binding. *Proteins* **78,** 2459–2468
67. Grzesiek, S., Stahl, S. J., Wingfield, P. T., and Bax, A. (1996) The CD4 determinant for downregulation by HIV-1 Nef directly binds to Nef. Mapping of the Nef binding surface by NMR. *Biochemistry* **35,** 10256–10261
68. Armougom, F., Moretti, S., Poirot, O., Audic, S., Dumas, P., Schaeli, B., Keduas, V., and Notredame, C. (2006) Expresso. Automatic incorporation of structural information in multiple sequence alignments using 3D-Coffee. *Nucleic Acids Res.* **34,** W604–W608